

On the Mean Square Error Optimal Estimator in One-Bit Quantized Systems

Benedikt Fesl, Michael Koller, and Wolfgang Utschick, *Fellow, IEEE*

Abstract—This paper investigates the mean square error (MSE)-optimal conditional mean estimator (CME) in one-bit quantized systems in the context of channel estimation with jointly Gaussian inputs. We analyze the relationship of the generally nonlinear CME to the linear Bussgang estimator, a well-known method based on Bussgang’s theorem. We highlight a novel observation that the Bussgang estimator is equal to the CME for different special cases, including the case of univariate Gaussian inputs and the case of multiple observations in the absence of additive noise prior to the quantization. For the general cases we conduct numerical simulations to quantify the gap between the Bussgang estimator and the CME. This gap increases for higher dimensions and longer pilot sequences. We propose an optimal pilot sequence, motivated by insights from the CME, and derive a novel closed-form expression of the MSE for that case. Afterwards, we find a closed-form limit of the MSE in the asymptotically large number of pilots regime that also holds for the Bussgang estimator. Lastly, we present numerical experiments for various system parameters and for different performance metrics which illuminate the behavior of the optimal channel estimator in the quantized regime. In this context, the well-known stochastic resonance effect that appears in quantized systems can be quantified.

Index Terms—Bussgang theorem, channel estimation, conditional mean estimation, one-bit quantization, mean square error.

I. INTRODUCTION

DIGITAL signal processing has great impact on modern communication systems, in which the analog signals undergo quantization through analog-to-digital converters (ADCs). The resolution of the ADCs determines how much information is preserved after the quantization of the analog signal. In many applications, the extreme case of one-bit quantization is of particular interest, e.g., in the context of lossy compression and rate distortion theory [1]. In recent years, one-bit quantization gained a lot of interest in multiple-input multiple-output (MIMO) communication systems, where transmitter and receiver are possibly equipped with a large number of antennas. Since the power consumption of the ADCs, which are needed for every antenna, is growing exponentially with their resolution, one-bit ADCs are considered as a power-efficient solution [2]. A major drawback of a system with one-bit ADCs is the severe information loss which diminishes the capacity [3]–[8]

and achievable rate [9], [10], and causes signal processing tasks like channel estimation to become challenging [11]–[13]. However, in contrast to multi-bit considerations, the study of one-bit quantization allows for closed-form solutions in many applications which we discuss in the following. Thereafter, the found exact solutions can be leveraged to approximate solutions for higher resolutions.

Remarkably, it is shown in [3], [4] that the capacity is not severely reduced by the coarse quantization at low signal-to-noise ratios (SNRs). The capacity was further analyzed for high SNRs in [5] and for a large number of antennas in [6]. In [9], [10], the achievable uplink throughput and rate is discussed. In order to achieve high data rates in quantized systems, accurate estimation of the channel state information (CSI) is particularly important. In consideration of the highly nonlinear quantization, channel estimation is considerably more demanding, leading to an extensive collection of approaches in the literature, e.g., [8], [14]–[29]. The work in [8] studies least squares (LS) estimation. In [14]–[17], iterative maximum likelihood (ML) methods are proposed, whereas in [18]–[20], the maximum a posteriori (MAP) estimator is analyzed. In [18], [21] the Cramér-Rao bound (CRB) is investigated. In [20], [22]–[24], compressive sensing (CS) is studied for channel estimation, and deep learning approaches were investigated in [25]–[29].

Apart from that, the Bussgang theorem turned out to be helpful for channel estimation [30]. The theorem, a special case of the more general Price theorem [31], states that the auto-correlation and cross-correlation of a zero-mean Gaussian signal before and after it has passed through a nonlinear operation is equal up to a constant. A direct consequence of the theorem is the fact that the signal after the quantization can be decomposed in a linear fashion into a desired signal part and an uncorrelated distortion. This property was investigated for various nonlinearities [32] and further extended to non-zero quantization thresholds [33]. In the context of signal processing, the theorem was successfully used to design channel estimators. To this end, the linearized model is combined with the linear minimum mean square error (MMSE) estimator [34]–[37].

Despite this extensive variety of channel estimation algorithms, there is so far no detailed discussion about the CME for the one-bit quantization case. The CME is well-known to be the minimizer for the MSE loss function, which is the most frequently considered criterion for the channel estimation performance. More generally, the CME is the optimal predictor for all Bregman loss functions, of which the MSE is a special case [38]. On the one hand, there are approximations of the

Benedikt Fesl and Michael Koller are with Professur für Methoden der Signalverarbeitung, Technische Universität München, 80333 München, Germany (e-mail: benedikt.fesl@tum.de; michael.koller@tum.de).

Wolfgang Utschick is with Professur für Methoden der Signalverarbeitung, Technische Universität München, 80333 München, Germany (e-mail: utschick@tum.de) and with the Munich Data Science Institute (MDSI).

CME, e.g., in wideband systems with many channel taps and antennas where the quantization noise becomes approximately Gaussian [39], or with neural networks that are trained on unquantized data [26]. On the other hand, the CME is known for the simple one-dimensional case for a Gaussian input without an observation matrix [1, Chapter 13.1], [40]. However, to our knowledge, there exists no general discussion about the multivariate case with correlated channel entries, or with pilot sequences that can not be optimally decorrelated.

In [37], a two-stage (concatenated) MMSE estimator is proposed, where in the first stage the product of the observation matrix and the channel is estimated with the CME. Afterwards, it is assumed that the remaining error is Gaussian, which is unlikely to hold in general, such that the channel can be recovered by decorrelating with the (pseudo-)inverse observation matrix. This corresponds to a second stage consisting of a linear MMSE solution. Interestingly, the two-stage approach is shown to be equal to the Bussgang estimator in the one-bit quantization case.

A. Contributions

We discuss the CME in systems with one-bit quantization for the general case of multivariate Gaussian channels in the presence of additive white Gaussian noise (AWGN) and multiple pilot observations. We present closed-form solutions for special cases and numerical computations for the general case. In that respect, we discuss the optimal pilot sequence from the perspective of the CME that was independently suggested in [26] for learning a neural network based channel estimator. We identify cases in which the Bussgang estimator is equivalent to the CME by proving that their closed-form MSE expressions are equal and we find asymptotic MSE limits for the large number of pilots regime. We then quantify the gap between the linear Bussgang estimator and the nonlinear CME in the general case by numerical experiments and show that the gap increases for higher dimensions and longer pilot sequences in the presence of correlations between the channel entries. In this context, the well-known stochastic resonance effect [41], which allows for outperforming the asymptotic limits in the presence of noise, is numerically quantified. We finally discuss further performance metrics such as the cosine similarity and a bound on the achievable rate for a matched filter.

The remainder of this work is structured as follows. In Section II, the problem formulation is described, in Section III, the Bussgang estimator is summarized, and in Section IV, the findings on the CME are presented. Section V then discusses further performance metrics, Section VI presents the numerical results, and Section VII concludes the work.

Notation: The (element-wise) signum function is denoted by $\text{sign}(\cdot)$. The Kronecker product is denoted by \otimes and the trace of matrix is written as $\text{tr}(\cdot)$. The real and imaginary part of a complex scalar/vector/matrix is stated as $\Re(\cdot)$ and $\Im(\cdot)$, respectively. The (column-wise) vectorization of a matrix which stacks the columns is denoted by $\text{vec}(\cdot)$. We denote the probability density function (PDF) of a continuous random variable (RV) x as f_x and the

probability mass function (PMF) of a discrete RV y as p_y . We denote the circularly symmetric complex Gaussian distribution with mean $\boldsymbol{\mu}$ and covariance \mathbf{C} , evaluated at \mathbf{x} , as $\mathcal{N}_{\mathbb{C}}(\mathbf{x}; \boldsymbol{\mu}, \mathbf{C})$. Similarly, the real-valued Gaussian density is denoted by $\mathcal{N}(\mathbf{x}; \mathbf{0}, \mathbf{C}_h)$. We denote the Gaussian error function as $\text{erf}(x) = \frac{2}{\sqrt{\pi}} \int_0^x \exp(-t^2) dt$. We denote the uniform distribution between a and b as $\mathcal{U}(a, b)$. The k, ℓ th entry of a matrix \mathbf{X} is denoted by $[\mathbf{X}]_{k, \ell}$.

II. PROBLEM FORMULATION

We consider the following generic system equation

$$\mathbf{R} = Q(\mathbf{Y}) = Q(\mathbf{h}\mathbf{a}^T + \mathbf{N}) \in \mathbb{C}^{N \times M} \quad (1)$$

where $\mathbf{R} = [\mathbf{r}_1, \mathbf{r}_2, \dots, \mathbf{r}_M]$ contains M quantized observations of the vector of interest $\mathbf{h} \in \mathbb{C}^N$ with the known observation vector $\mathbf{a} \in \mathbb{C}^M$ that fulfills the power constraint $\|\mathbf{a}\|_2^2 = M$. We denote by \mathbf{Y} the unquantized received signal. Let the vector \mathbf{h} be a zero-mean Gaussian RV, i.e., $\mathbf{h} \sim \mathcal{N}_{\mathbb{C}}(\mathbf{0}, \mathbf{C}_h)$. The desired signal is distorted with additive zero-mean Gaussian noise $\mathbf{N} = [\mathbf{n}_1, \mathbf{n}_2, \dots, \mathbf{n}_M]$ where $\mathbf{n}_i \sim \mathcal{N}_{\mathbb{C}}(\mathbf{0}, \mathbf{C}_n)$ and is afterwards quantized with the complex-valued one-bit quantization function

$$Q(\cdot) = \frac{1}{\sqrt{2}} (\text{sign}(\Re(\cdot)) + j \text{sign}(\Im(\cdot))) \quad (2)$$

which is applied element-wise to the input vector/matrix. The system model in (1) can be equivalently described in its (column-wise) vectorized form as

$$\mathbf{r} = Q(\mathbf{y}) = Q(\mathbf{A}\mathbf{h} + \mathbf{n}) \in \mathbb{C}^{NM} \quad (3)$$

with $\mathbf{A} = \mathbf{a} \otimes \mathbf{I}$, $\mathbf{r} = \text{vec}(\mathbf{R})$, $\mathbf{y} = \text{vec}(\mathbf{Y})$, and $\mathbf{n} = \text{vec}(\mathbf{N})$. The system model describes, e.g., a single-input multiple-output (SIMO) wireless communication scenario where a base station equipped with N antennas receives M pilot signals from a single-antenna user terminal. The ADCs at the receiver have one-bit resolution, which is modeled by the quantization function in (2). However, the analysis in this work is not limited to this instance.

The overall goal is to estimate the signal \mathbf{h} in an optimal sense where the vector \mathbf{a} is known and the channel and noise are both zero-mean Gaussian with known covariances. The optimality depends on the metric of choice, however, the most frequently used criterion in the context of channel estimation is the MSE between the true channel \mathbf{h} and its estimate $\hat{\mathbf{h}}$, i.e.,

$$\text{MSE} = \mathbb{E}[\|\mathbf{h} - \hat{\mathbf{h}}\|_2^2] \quad (4)$$

for which the CME, defined as

$$\hat{\mathbf{h}} = \mathbb{E}[\mathbf{h} | \mathbf{r}] = \int \mathbf{h} f_{\mathbf{h}|\mathbf{r}}(\mathbf{h} | \mathbf{r}) d\mathbf{h}, \quad (5)$$

is known to yield optimal estimates. The CME is generally not available since it requires full knowledge of the conditional PDF $f_{\mathbf{h}|\mathbf{r}}$. Furthermore, even if the PDF is known, the CME does generally neither have a closed-form solution nor is it feasible to compute numerically in real-time systems. For this reason, the CME is usually approximated by sub-optimal approaches with a practically reasonable trade-off between

performance and complexity, e.g., using the linear MMSE estimator. In a jointly Gaussian setting, the linear MMSE estimator is well-known to be the CME. However, in the quantized case, this statement is no longer true in general. Nonetheless, for a zero-mean jointly Gaussian input, the Bussgang decomposition, based on Bussgang's theorem [30], can be leveraged to design a linear MMSE estimator in the quantized case. The Bussgang estimator is sub-optimal in general due to its linearity. However, up to now there has been no analysis of the connection between the Bussgang estimator and the CME in the case of one-bit quantization.

In this work, we investigate the MSE optimality of the Bussgang estimator and identify cases in which the Bussgang estimator is equal to the CME and we show when the Bussgang estimator differs from the CME. To this end, after revising the Bussgang estimator, we derive the CME for one-bit quantization in the multivariate case. Simulation results based on the derived quantities verify the discussion.

III. BUSSGANG ESTIMATOR

In this section, we briefly revise the linear MMSE estimator based on the Bussgang decomposition which is a direct consequence of Bussgang's theorem [30]. In particular, the Bussgang decomposition implies that the system in (3) can be written as a linear combination of the desired signal part and an uncorrelated distortion \mathbf{q} as

$$\mathbf{r} = Q(\mathbf{y}) = \mathbf{B}\mathbf{y} + \boldsymbol{\eta} = \mathbf{B}\mathbf{A}\mathbf{h} + \mathbf{q}, \quad (6)$$

where \mathbf{B} is the Bussgang gain that can be obtained from the linear MMSE estimation of \mathbf{r} from \mathbf{y} as

$$\mathbf{B} = \mathbf{C}_{\mathbf{r}\mathbf{y}}\mathbf{C}_{\mathbf{y}}^{-1} = \sqrt{\frac{2}{\pi}} \text{diag}(\mathbf{C}_{\mathbf{y}})^{-\frac{1}{2}}, \quad (7)$$

cf. [42, Chapter 9-2], and where the distortion term $\mathbf{q} = \mathbf{B}\mathbf{n} + \boldsymbol{\eta}$ contains both the AWGN \mathbf{n} and the quantization noise $\boldsymbol{\eta}$. As the statistically equivalent model (6) is linear, one can formulate the linear MMSE estimator

$$\hat{\mathbf{h}}_{\text{buss}} = \mathbf{C}_{\mathbf{h}\mathbf{r}}\mathbf{C}_{\mathbf{r}}^{-1}\mathbf{r}. \quad (8)$$

The cross-correlation matrix between the channel and the received signal is calculated as

$$\mathbf{C}_{\mathbf{h}\mathbf{r}} = \mathbb{E}[\mathbf{h}(\mathbf{B}\mathbf{A}\mathbf{h} + \mathbf{q})^{\text{H}}] = \mathbf{C}_{\mathbf{h}}\mathbf{A}^{\text{H}}\mathbf{B}^{\text{H}} \quad (9)$$

which follows from the fact that the noise term \mathbf{q} is uncorrelated with the channel. The auto-correlation matrix $\mathbf{C}_{\mathbf{r}}$ is calculated via the so-called arcsine law [43] as

$$\mathbf{C}_{\mathbf{r}} = \frac{2}{\pi} (\arcsin(\boldsymbol{\Psi}\Re(\mathbf{C}_{\mathbf{y}})\boldsymbol{\Psi}) + j \arcsin(\boldsymbol{\Psi}\Im(\mathbf{C}_{\mathbf{y}})\boldsymbol{\Psi})) \quad (10)$$

where $\boldsymbol{\Psi} = \text{diag}(\mathbf{C}_{\mathbf{y}})^{-\frac{1}{2}}$. Further reading on the Bussgang estimator can be found in [9], [34].

In [37], it is discussed that the Bussgang estimator is equal to a two-stage estimator that first computes the CME of the product $\mathbf{A}\mathbf{h}$ of channel and observation matrix, and afterwards recovers the channel \mathbf{h} . Since the resulting error after the first step is non-Gaussian, the second step is non-optimal from the CME perspective. In the following, we discuss cases in which the Bussgang estimator is indeed equal to the CME, and we show the differences between the CME and the Bussgang estimator in the general case.

IV. CONDITIONAL MEAN ESTIMATOR

In this section, we derive the CME for one-bit quantization for the general system in (3). Afterwards, we discuss the CME for different simplifications, i.e., with and without AWGN or multiple pilots, and for the uni- as well as multivariate case, where these cases are differently combined to provide a general overview. For each instance, we discuss possible closed-form solutions of the CME and its relationship to the Bussgang estimator, where we identify cases in which equality between these estimators holds. We start by rewriting the CME from (5) as

$$\mathbb{E}[\mathbf{h} | \mathbf{r}] = \int \mathbf{h} \frac{p_{\mathbf{r}|\mathbf{h}}(\mathbf{r}|\mathbf{h})f_{\mathbf{h}}(\mathbf{h})}{p_{\mathbf{r}}(\mathbf{r})} d\mathbf{h} \quad (11)$$

$$= \frac{1}{p_{\mathbf{r}}(\mathbf{r})} \int \mathbf{h} f_{\mathbf{h}}(\mathbf{h}) p_{\mathbf{r}|\mathbf{h}}(\mathbf{r}|\mathbf{h}) d\mathbf{h} \quad (12)$$

by making use of Bayes' theorem. It is known that $f_{\mathbf{h}} = \mathcal{N}_{\mathbb{C}}(\mathbf{0}, \mathbf{C}_{\mathbf{h}})$. In the following, we also find expressions for the prior and conditional probabilities. We first define the set of all vectors \mathbf{y} which are mapped onto a given observation \mathbf{r} as

$$\bar{Q}(\mathbf{r}) = \{\mathbf{y} \in \mathbb{C}^{MN} : Q(\mathbf{y}) = \mathbf{r}\}. \quad (13)$$

Integrating the PDF $f_{\mathbf{y}}$ over this set yields the prior probability of observing the respective quantized observation, i.e.,

$$p_{\mathbf{r}}(\mathbf{r}) = \int_{\bar{Q}(\mathbf{r})} f_{\mathbf{y}}(\mathbf{y}) d\mathbf{y}, \quad (14)$$

where due to the joint Gaussianity we have $f_{\mathbf{y}} = \mathcal{N}_{\mathbb{C}}(\mathbf{0}, \mathbf{C}_{\mathbf{y}})$ with $\mathbf{C}_{\mathbf{y}} = \mathbf{A}\mathbf{C}_{\mathbf{h}}\mathbf{A}^{\text{H}} + \mathbf{C}_{\mathbf{n}}$, cf. (3). The conditional probability $p_{\mathbf{r}|\mathbf{h}}(\mathbf{r}|\mathbf{h})$ is found similarly, however, now the integrand changes to $\mathcal{N}_{\mathbb{C}}(\mathbf{A}\mathbf{h}, \mathbf{C}_{\mathbf{n}})$, where \mathbf{h} is no longer a RV:

$$p_{\mathbf{r}|\mathbf{h}}(\mathbf{r}|\mathbf{h}) = \int_{\bar{Q}(\mathbf{r})} \mathcal{N}_{\mathbb{C}}(\mathbf{x}; \mathbf{A}\mathbf{h}, \mathbf{C}_{\mathbf{n}}) d\mathbf{x}. \quad (15)$$

Plugging (14) and (15) into (12) yields a generally computable expression of the CME for the model in (3).

A. Numerical Integration

For the most general case, the integrals in (12), (14), and (15) do neither have a closed-form solution, nor can they be simplified. In this case, the CME has to be found by numerical integration. However, the number of solutions for the discrete number of possible observations $\mathbf{r} \in \mathbb{C}^{MN}$ grows exponentially with 4^{MN} , not to mention the increasing complexity for each individual solution. Since in (14) and (15) we have integrals over Gaussian PDFs, there exist computationally efficient algorithms. In this paper, the numerical integration of the Gaussian density is based on an algorithm from [44] which first transforms the integral into an integration over the unit hypercube by combining a Cholesky decomposition of the covariance matrix with a priority ordering of the integration variables. The transformed integral is then approximated based on a Monte Carlo method which is implemented in [45]. In the following, we discuss special instances of the general model (3) that allow for a simplified computation of the CME (12).

B. Univariate Case with a Single Observation

In the following, the case of a scalar $N = 1$ system with a single observation $M = 1$, i.e., $a = 1$, is considered. Since the quantization function in (2) is applied independently to the real and imaginary part of its input, deriving only the real part formula of the CME is sufficient here since the imaginary part is computed analogously. To this end we consider $h_{\Re} \sim \mathcal{N}(0, \sigma^2)$, $n_{\Re} \sim \mathcal{N}(0, \eta^2)$, and for the ease of notation we define $r_{\Re} = \text{sign}(h_{\Re} + n_{\Re})$.

Because of the symmetry of the zero-mean Gaussian density, we get $p_{r_{\Re}}(r_{\Re}) = 1/2$. Furthermore, the integral in (15) can be computed in closed-form to

$$p_{r_{\Re}|h_{\Re}}(r_{\Re} = 1|h_{\Re}) = \int_0^{\infty} \mathcal{N}(x; h_{\Re}, \eta^2) dx \quad (16)$$

$$= \frac{1}{2} \left(1 + \text{erf} \left(\frac{h_{\Re}}{\sqrt{2}\eta} \right) \right), \quad (17)$$

$$p_{r_{\Re}|h_{\Re}}(r_{\Re} = -1|h_{\Re}) = \int_{-\infty}^0 \mathcal{N}(x; h_{\Re}, \eta^2) dx \quad (18)$$

$$= \frac{1}{2} \left(1 - \text{erf} \left(\frac{h_{\Re}}{\sqrt{2}\eta} \right) \right). \quad (19)$$

We can summarize (17) and (19) as

$$p_{r_{\Re}|h_{\Re}}(r_{\Re}|h_{\Re}) = \frac{1}{2} \left(1 + r_{\Re} \text{erf} \left(\frac{h_{\Re}}{\sqrt{2}\eta} \right) \right). \quad (20)$$

Plugging this result into (12) yields

$$\mathbb{E}[h_{\Re} | r_{\Re}] = \int_{-\infty}^{\infty} h f_h(h) \left(1 + r_{\Re} \text{erf} \left(\frac{h}{\sqrt{2}\eta} \right) \right) dh \quad (21)$$

$$= \sqrt{\frac{2}{\pi}} \frac{\sigma^2}{\sqrt{\sigma^2 + \eta^2}} r_{\Re}. \quad (22)$$

This can now easily be extended to the complex case with $h \sim \mathcal{N}_{\mathbb{C}}(0, \sigma^2)$, $n \sim \mathcal{N}_{\mathbb{C}}(0, \eta^2)$, and $r = Q(h + n)$ which then reads as

$$\mathbb{E}[h | r] = \frac{1}{\sqrt{\pi}} \frac{\sigma^2}{\sqrt{\sigma^2 + \eta^2}} r. \quad (23)$$

The closed-form MSE from (4) is then computed to

$$\text{MSE} = \sigma^2 \left(1 - \frac{2}{\pi} \frac{\sigma^2}{\sigma^2 + \eta^2} \right). \quad (24)$$

Interestingly, if we evaluate the Bussgang estimator in (8), we get the exact same CME and MSE expression. To conclude, for this case the Bussgang estimator is indeed the CME. Note that in the multivariate case with an identity observation matrix $\mathbf{A} = \mathbf{I}$ and uncorrelated channels $\mathbf{C}_h = \text{diag}(\mathbf{c}_h)$ as well as uncorrelated noise $\mathbf{C}_n = \text{diag}(\mathbf{c}_n)$, the PDFs in (14) and (15) can be decomposed into the product of their marginals. Thus, the CME from (23) can be applied element-wise and is therefore also equal to the Bussgang estimator. The same expression as in (23) was found in [40], more generally for non zero-mean channels. However, the Bussgang theorem from [30] can not be applied for non zero-mean RVs and thus, the equality does not hold in general.

Additionally, we can evaluate the well-known linear MMSE estimator for unquantized observations where it is the CME. There, the closed-form MSE is simply

$$\text{MSE} = \sigma^2 \left(1 - \frac{\sigma^2}{\sigma^2 + \eta^2} \right). \quad (25)$$

We can now compute the necessary SNR for the unquantized system to achieve the same MSE as the one-bit quantized system without AWGN which we will analyze later in the numerical experiments section.

C. Multivariate Noiseless Case with a Single Observation

In this case, we consider $M = 1$ with $\mathbf{n} = \mathbf{0}$. Similarly as in Section IV-B, it is sufficient to derive only the real part of the CME. To this end, we consider $\mathbf{r}_{\Re} = \text{sign}(\mathbf{h}_{\Re})$ with $\mathbf{h}_{\Re} \sim \mathcal{N}(\mathbf{0}, \mathbf{C}_h)$ where $\mathbf{C}_h \in \mathbb{R}^{N \times N}$ is a full matrix. We abuse the notation for $\overline{Q}(\mathbf{r}_{\Re}) = \{\mathbf{h}_{\Re} \in \mathbb{R}^N : \text{sign}(\mathbf{h}_{\Re}) = \mathbf{r}_{\Re}\}$. In the following Proposition 1, a simplified expression of the general CME (12) is derived whose advantage is discussed afterwards.

Proposition 1. *The CME for the above system can be computed element-wise as*

$$\mathbb{E}[\mathbf{h}_{\Re} | \mathbf{r}_{\Re}]_i = \frac{1}{p_{r_{\Re}}(\mathbf{r}_{\Re})} \sum_{n=1}^N [\mathbf{r}_{\Re}]_n [\mathbf{C}_h]_{i,n} \quad (26)$$

$$\mathcal{N}(0; 0, [\mathbf{C}_h]_{n,n}) \int_{\overline{Q}(\mathbf{r}_{\Re})} \mathcal{N}^n(\mathbf{x}; \mathbf{0}, \mathbf{C}_h) d\mathbf{x},$$

where $\mathcal{N}^n(\mathbf{0}, \mathbf{C}_h)$ is the $(N - 1)$ -dimensional Gaussian PDF where the n th row and column of \mathbf{C}_h^{-1} is deleted. The superscript n of a vector truncates its n th element.

Proof: See Appendix A.

The advantage of the integral in (26) is that, in contrast to the double integral that appears in (12), cf. (15), it can be efficiently computed by means of [44] as described in Section IV-A because there appear only integrals over Gaussian PDFs. Note that the expression (26) simplifies to the element-wise CME as computed in (23) for diagonal covariances since then $[\mathbf{C}_h]_{i,n}^{i \neq n} = 0$ and the $(N - 1)$ -dimensional integral equals $2^{-(N-1)}$ due to symmetry. This analysis can be interpreted as an asymptotic SNR analysis in which the AWGN goes to zero.

In contrast to the univariate case in Section IV-B, the resulting CME expression (26) is nonlinear and no longer in closed-form, which is clearly a difference to the linear Bussgang estimator. We will present numerical evaluations for this case that reveal a performance gap between the estimators.

D. Univariate Noiseless Case with Multiple Observations

In this case, we consider $N = 1$ with $\mathbf{n} = \mathbf{0}$, i.e., the system from (3) simplifies to $\mathbf{r} = Q(\mathbf{a}h)$ with $h \sim \mathcal{N}_{\mathbb{C}}(0, \sigma^2)$. Note that in this case it is not sufficient to compute the real-valued CME because of the product of channel and pilot vector. This was the reason for the two-stage approach in [37]. Opposite to the unquantized case, having multiple observations of the same realization is helpful in the context of quantization as more information can be recovered. Because the amplitude of

the received signal is lost after the one-bit quantizer, having varying amplitude in the pilot sequence \mathbf{a} has no influence on the observed signal. However, one can introduce phase shifts in order to increase the obtained information.

In the following, we discuss the optimal pilot sequence and the CME based thereon. With the quantization function in (2) there are four possible quantization labels in the complex plane for each observation. In the case of $M = 1$, the conditional PDF $p_{r|h}$ is an indicator function of a quadrant in the complex plane, cf. (43) for the multivariate real-valued case. Consequently, with M observations, the support of the conditional PDF $p_{r|h}$ can be divided into $4M$ regions. In order to identify the shape of these regions we make use of the following properties. First, the input RV has a zero-mean Gaussian PDF which is symmetric about the origin. Second, the amplitude information is lost due to the one-bit quantization. From these properties we deduce that all $4M$ regions have to be circular sectors centered at the origin with the same angle of $\frac{\pi}{2M}$. Consequently, we define the indicator function

$$p_{r|h}(\mathbf{r}|h) = \begin{cases} 1 & h \in \mathcal{Q}(\mathbf{r}) \\ 0 & h \notin \mathcal{Q}(\mathbf{r}) \end{cases} \quad (27)$$

where $\mathcal{Q}(\mathbf{r})$ is a circular sector

$$\mathcal{Q}(\mathbf{r}) = \left\{ \alpha e^{j\theta} \in \mathbb{C} : \alpha \in \mathbb{R}_+, \phi(\mathbf{r}) \leq \theta < \phi(\mathbf{r}) + \frac{\pi}{2M} \right\} \quad (28)$$

whose boundary angle ϕ is a function of \mathbf{r} . An optimal choice of the pilot sequence allows us to identify in which of the circular sectors the channel lies based on the received sequence of quantized observations. We find a pilot sequence that fulfills this condition by shifting each transmitted signal successively by an angle of $\frac{\pi}{2M}$, i.e.,

$$[\mathbf{a}]_m = \exp\left(j\frac{\pi}{2M}(m-1)\right), \quad m = 1, \dots, M. \quad (29)$$

Note that $||[\mathbf{a}]_m|^2 = 1$ in order to fulfill the power constraint and $[\mathbf{a}]_1 = 1$ such that the first pilot has no phase shift. Interestingly, the same pilot sequence was proposed in [26] with the purpose to achieve a bijective mapping between a fixed dataset of channels and corresponding observations with long enough pilot sequences.

An intuitive explanation on how the circular sector of interest (28) can be identified with the proposed pilot sequence (29) is given by the following example. Fig. 1 shows the case of $M = 3$ observations with two different transmission examples. The blue and red dots illustrate the unquantized pilot sequence before the quantization. Each dot is mapped to its nearest quantization label q_i . For pilot sequence one, the same quantization label q_1 is received for each observation, and because of the introduced phase shifts, the channel h must lie in the blue vertically lined circular sector. If it would lie in its neighboring circular sector, either the first or last observation would be quantized to a different label. For pilot sequence two, the labels $\mathbf{r} = [q_1, q_2, q_2]$ are received. Since the quantization label shifts already after the first observation, the channel must lie in the respective red cross-hatched circular sector.

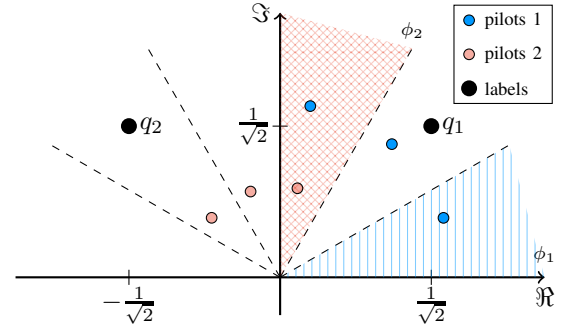


Fig. 1: Example of unquantized pilot sequences generated by (29) with $M = 3$ and corresponding circular sectors indicated by dashed lines. The blue lined (red cross-hatched) circular sector corresponds to the first (second) pilot sequence.

With the designed pilot sequence (29), we find the angle function ϕ from (28) as

$$\phi(\mathbf{r}) = \frac{1}{M} \sum_{m=1}^M \angle([\mathbf{r}]_m) - \frac{\pi}{4} \quad (30)$$

where $\angle(\cdot)$ gives the angle of a complex number in $[0, 2\pi)$. For the example in Fig. 1, for pilot sequence one, $\phi(\mathbf{r}) = 0$, and for pilot sequence two we get $\phi(\mathbf{r}) = \frac{\pi}{3}$. Note that the pilot sequence (29) is an ambiguous choice since a constant phase offset can be introduced such that the resulting pilots still have the necessary properties when adapting the angle function ϕ from (30). With these preparations, we can now find a closed-form solution for the CME.

Proposition 2. *The CME for the above system is computed to*

$$\mathbb{E}[h | \mathbf{r}] = \frac{2M\sigma}{\sqrt{\pi}} \sin\left(\frac{\pi}{4M}\right) \exp\left(j\left(\frac{\pi}{4M} + \phi(\mathbf{r})\right)\right). \quad (31)$$

Proof: See Appendix B.

The closed-form MSE for the CME from (31) is then

$$\text{MSE} = \sigma^2 \left(1 - \frac{4M^2}{\pi} \sin^2\left(\frac{\pi}{4M}\right)\right). \quad (32)$$

In contrast, the MSE for the Bussgang estimator from (8) for the present system is computed to

$$\text{MSE} = \sigma^2 \left(1 - \frac{2}{\pi} \mathbf{a}^H \mathbf{C}_r^{-1} \mathbf{a}\right). \quad (33)$$

Although the MSE terms in (32) and (33) seem to be different, we show their equality in the following.

Proposition 3. *The MSE of the Bussgang estimator from (33) is equal to the MSE of the CME from (32) for an arbitrary number of observations.*

Proof: See Appendix C.

Proposition 3 surprisingly shows that the linear Bussgang estimator achieves the same MSE as the CME and is thus a MSE-optimal estimator for that case. Interestingly, as a byproduct of the proof in Appendix C we have found a closed-form expression for the inverse covariance matrix \mathbf{C}_r^{-1} in (33). Yet again, this case can be interpreted as an asymptotically

Dim. N	AWGN	Corr.	Pilots M	Optimal
≥ 1	no	no	≥ 1	yes
≥ 1	yes	no	1	yes
≥ 1	yes	no	> 1	no
> 1	no/yes	yes	≥ 1	no

TABLE I: Overview of different system parameters and the MSE-optimality of the Bussgang estimator.

high SNR analysis. It should be noted here that a similar proof is not possible in the presence of AWGN which we will show during numerical experiments later. With the closed-form MSE expression in (32), we can now study the asymptotically large number of pilots regime where we find the following result which, due to Proposition 3, also holds for the Bussgang estimator.

Proposition 4. For $M \rightarrow \infty$ the MSE from (32) is

$$\lim_{M \rightarrow \infty} \text{MSE} = \sigma^2 \left(1 - \frac{\pi}{4}\right). \quad (34)$$

Proof. We compute

$$\lim_{M \rightarrow \infty} M \sin\left(\frac{\pi}{4M}\right) = \lim_{M \rightarrow \infty} \frac{\pi}{4} \cos\left(\frac{\pi}{4M}\right) = \frac{\pi}{4} \quad (35)$$

where the rule of L'Hôpital was used. Since this limit exists, we can conclude that

$$\lim_{M \rightarrow \infty} M^2 \sin^2\left(\frac{\pi}{4M}\right) = \frac{\pi^2}{16}. \quad (36)$$

Plugging (36) into (32) verifies (34). \square

E. Summary

So far, we have discussed the CME and its relationship to the Bussgang estimator for different system instances. Remarkably, in Section IV-B and Section IV-D the Bussgang estimator is shown to be equal to the CME which has a closed-form. This is a novel result and has not been stated in the literature so far. Because of the closed-form MSE expression of the CME, an analysis of the large number of pilots regime was possible which resulted in a closed-form limit. What is more, we have discussed in Section IV-C that the equality might not hold for correlated channel entries, even in the absence of AWGN. However, we have derived a computationally efficient expression for the CME in that case.

An overview of the different cases where the Bussgang estimator is equal to the CME or not can be found in Table I. Therein, we show the cases where the Bussgang estimator is MSE-optimal with respect to the dimension (Dim.) N , the presence/absence of AWGN, the correlation (Corr.) between channel entries and the number of pilots/observations M .

In the following, after introducing different performance metrics besides the MSE, we discuss the above results in numerical experiments which verify the theoretical findings and quantify the gap between the Bussgang estimator and the CME for different system parameters.

V. DIFFERENT PERFORMANCE METRICS

A. Cosine Similarity

The amplitude of the received signal is lost due to the one-bit quantization. For this reason, one might solely be interested in how well an estimator can recover the angle of the signal of interest. A measure for the difference of the angle ψ between the true and estimated channel is the *cosine similarity* which we define as

$$\cos \psi = \frac{\Re(\mathbf{h}^H \hat{\mathbf{h}})}{\|\mathbf{h}\| \|\hat{\mathbf{h}}\|}. \quad (37)$$

Note that the cosine similarity lies between -1 (opposite direction) and 1 (same direction).

B. Achievable Rate Lower Bound

The achievable rate is of great interest in quantized systems [9], [10]. For our considerations, we are aiming at a comparison between the CME and the Bussgang estimator via the corresponding achievable rate of a respective data transmission system that is taking the CSI mismatch into account. To this end, after estimating the channel with the pilot transmission in (3), the data symbol s is transmitted over the same channel, i.e.,

$$\mathbf{w} = Q(\mathbf{h}s + \mathbf{n}) = \mathbf{B}\mathbf{h}s + \mathbf{q} \quad (38)$$

where in the second equation the linearized model with Bussgang's decomposition is used where $\mathbf{q} = \mathbf{B}\mathbf{n} + \boldsymbol{\eta}$. We make the worst-case assumption that the quantization noise is Gaussian, i.e., $\mathbf{q} \sim \mathcal{N}_C(\mathbf{0}, \mathbf{C}_r - \mathbf{B}\mathbf{C}_h\mathbf{B}^H)$, cf. [46], and use a matched filter

$$\mathbf{g}_{\text{MF}}^H = \hat{\mathbf{h}}^H \mathbf{B}^H (\mathbf{C}_r - \mathbf{B}\mathbf{C}_h\mathbf{B}^H)^{-1} \quad (39)$$

at the receiver. Note that here the variance of the data symbol s is assumed to be one without loss of generality. We further assume that the SNR is the same during pilot and data transmission. Thus, we can evaluate the achievable rate lower bound as

$$\begin{aligned} R &= \mathbb{E} \left[\log_2 \left(1 + \frac{|\mathbf{g}_{\text{MF}}^H \mathbf{B} \mathbf{h}|^2}{\mathbf{g}_{\text{MF}}^H (\mathbf{C}_r - \mathbf{B}\mathbf{C}_h\mathbf{B}^H) \mathbf{g}_{\text{MF}}} \right) \right] \quad (40) \\ &= \mathbb{E} \left[\log_2 \left(1 + \frac{|\hat{\mathbf{h}}^H \mathbf{B}^H (\mathbf{C}_r - \mathbf{B}\mathbf{C}_h\mathbf{B}^H)^{-1} \mathbf{B} \mathbf{h}|^2}{\hat{\mathbf{h}}^H \mathbf{B}^H (\mathbf{C}_r - \mathbf{B}\mathbf{C}_h\mathbf{B}^H)^{-1} \mathbf{B} \hat{\mathbf{h}}} \right) \right] \quad (41) \end{aligned}$$

with Monte Carlo simulations.

VI. NUMERICAL RESULTS

In this section, we perform numerical experiments that verify our theoretical derivations and allow for quantifying the performance gap between the Bussgang estimator and the CME in the general case. We consider a diagonal noise covariance $\mathbf{C}_n = \eta^2 \mathbf{I}$. For the case of $N = 1$, we choose without loss of generality the variance of the channel to $\sigma^2 = 1$. In the multivariate case, we randomly sample channel covariance matrices with the following procedure, cf. [47]. We first generate a matrix \mathbf{S} where $[\mathbf{S}]_{m,n} \sim \mathcal{U}(0,1)$. Then, we compute the eigenvalue decomposition (EVD) of $\mathbf{S}^H \mathbf{S} = \mathbf{V} \boldsymbol{\Sigma} \mathbf{V}^H$. Finally, we construct $\mathbf{C}_h = \mathbf{V} \text{diag}(\mathbf{1} + \boldsymbol{\xi}) \mathbf{V}^H$, where $[\boldsymbol{\xi}]_m \sim \mathcal{U}(0,1)$.

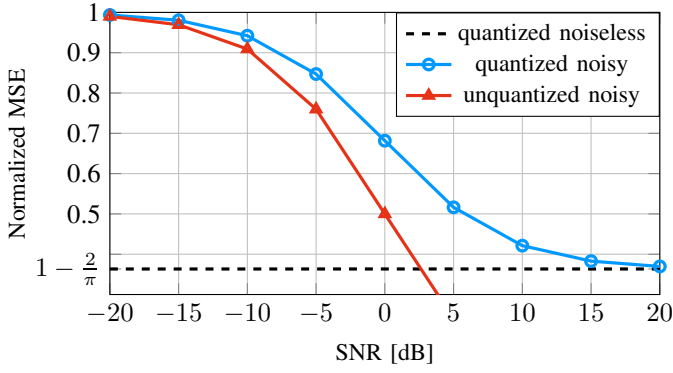


Fig. 2: MSE performance of the CME from Section IV-B for $N=M=1$ for unquantized and one-bit quantized observations.

Afterwards, we normalize each covariance matrix with its trace times the dimension N . For each covariance matrix we draw a single channel sample. This procedure averages out all possible structural features of the covariance matrix. For all simulations we draw a total of 10,000 samples. With the property $\|\mathbf{a}\|_2^2 = M$ and $E[\|\mathbf{h}\|^2] = N$ we define the SNR as

$$\text{SNR} = \frac{\|\mathbf{a}\|_2^2 E[\|\mathbf{h}\|^2]}{E[\|\mathbf{n}\|^2]} = \frac{1}{\eta^2}. \quad (42)$$

The MSE from (4) is normalized by $E[\|\mathbf{h}\|^2] = N$.

A. Univariate Case with a Single Observation

We first verify the findings from Section IV-B with $N = M = 1$ in Fig. 2 where the normalized MSE is plotted against the SNR. It can be observed that the CME converges to the noiseless MSE from (24) for $\eta = 0$, which equals to $1 - \frac{2}{\pi}$, for high SNR values. Additionally, we have plotted the well-known linear MMSE estimator for unquantized observation, where it is the CME, from (25). Comparing a one-bit quantized system without AWGN with an unquantized system, we can compute their MSE intersection point by means of (24) and (25) with the SNR definition (42) to $\text{SNR} = \frac{2}{\pi-2} \approx 2.435\text{dB}$ which is verified by the simulation.

B. Multivariate Noiseless Case with a Single Observation

Next, we discuss the system from Section IV-C with $M = 1$ and $\mathbf{n} = \mathbf{0}$. As discussed above, for this case there exists no closed-form solution, but we can use a computationally efficient algorithm from [44] to evaluate the integrals from (14) and (26). In Fig. 3 it can be seen that the normalized MSE decreases for larger dimensions N which is a consequence of the existing cross-correlations that are exploited for the estimation. Furthermore, the gap between the Bussgang estimator and the CME increases for higher dimensions. That is, the sub-optimality of the Bussgang estimator seems to have greater impact especially in higher dimensions. Note that in the case of $N = 1$ there exists the closed-form solution from before where the Bussgang estimator is exactly the CME.

Fig. 4 evaluates the cosine similarity from (37) over different dimensions N . For an increasing number of dimensions it can be seen that the cosine similarity generally decreases.

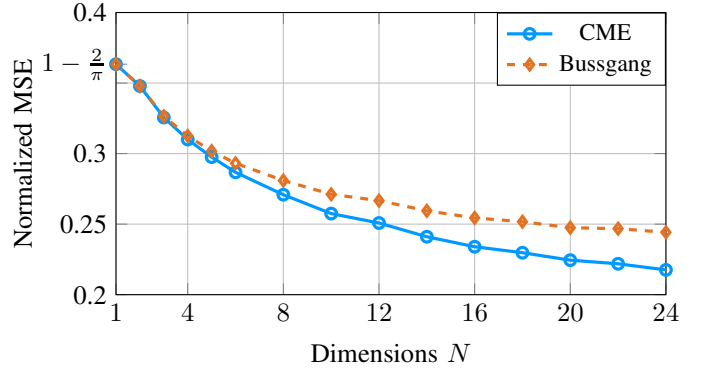


Fig. 3: MSE performance comparison between the Bussgang estimator and the CME from Section IV-C for the multivariate noiseless case with a single observation.

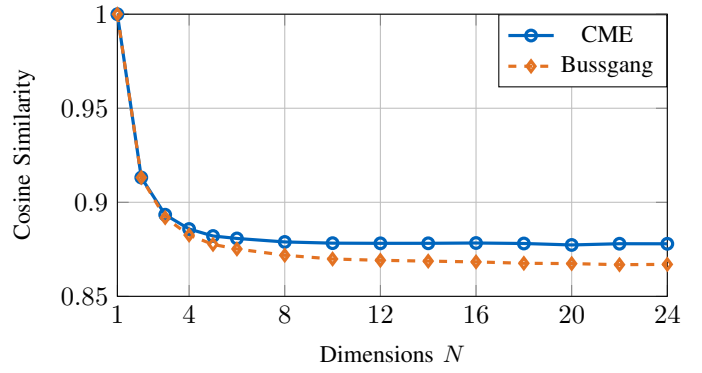


Fig. 4: Cosine similarity performance comparison between the Bussgang estimator and the CME from Section IV-C for the multivariate noiseless case with a single observation.

However, the CME achieves a higher cosine similarity than the Bussgang estimator with an increasing gap for higher dimensions where a saturation is observed. This is in accordance with the results from the MSE investigations.

In Fig. 5, we analyze the achievable rate lower bound from (41) in bits/s/Hz. Both estimators achieve a very similar rate which increases from around 1 bit/s/Hz for $N = 1$ up to over 4 bits/s/Hz for $N > 16$. Nevertheless, a slight performance gap between both estimators can be observed which we investigate further in the following.

In Fig. 6, we have evaluated the relative difference between the Bussgang estimator and the CME with respect to the number of dimensions for different performance criteria. For the MSE the relative difference increases from 0 for $N = 1$, where the equality of both estimators holds, to around 5% for $N = 10$, to over 10% for $N = 22$. The relative difference for the cosine similarity only goes up to approximately 1.2%, whereas for the achievable rate the relative difference is the smallest with only about 0.8% for $N = 24$. To conclude, although the MSE difference between the Bussgang estimator and the CME becomes quite substantial for larger dimensions, the relative difference is lower for the cosine similarity and the achievable rate lower bound where a saturation can be observed.

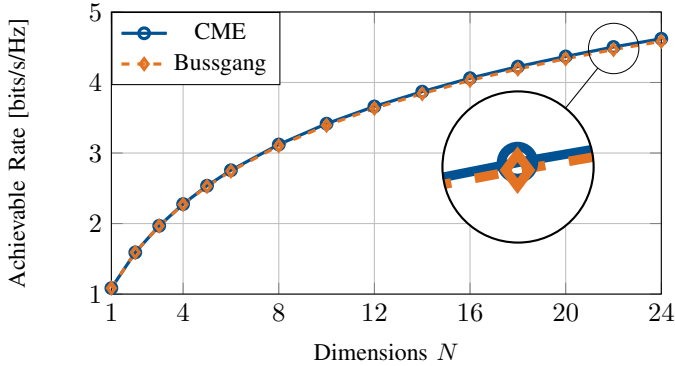


Fig. 5: Achievable rate lower bound comparison between the Bussgang estimator and the CME from Section IV-C for the multivariate noiseless case with a single observation.

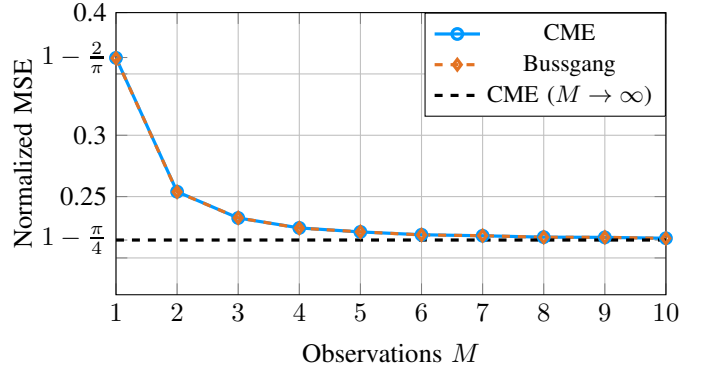


Fig. 7: MSE performance comparison between the Bussgang estimator and the CME from Section IV-D for the univariate noiseless case with multiple observations.

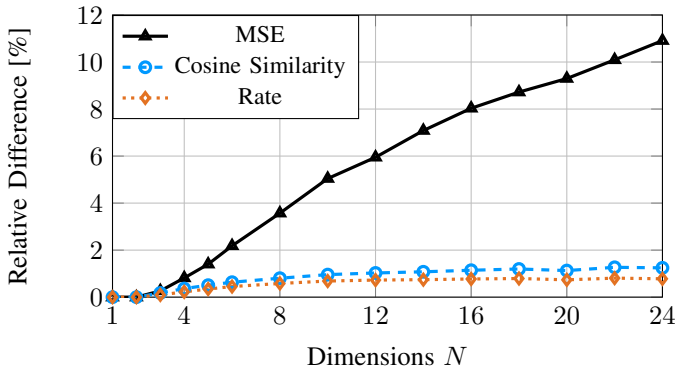


Fig. 6: Relative difference between the Bussgang estimator and the CME from Section IV-C for different performance metrics for the multivariate noiseless case with a single observation.

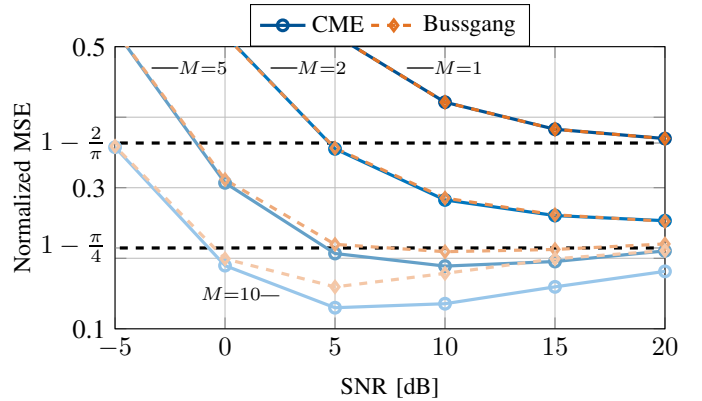


Fig. 8: MSE performance comparison between the Bussgang estimator and the CME from Section IV-A for the univariate case with multiple observations.

C. Univariate Noiseless Case with Multiple Observations

In this subsection, we evaluate the results from Section IV-D with $N = 1$ and $\mathbf{n} = \mathbf{0}$. Fig. 7 shows the normalized MSE over the number of pilots M . First, it can be seen that the MSE of the estimators in (8) and (31) are indeed equal for the conducted simulation, verifying Proposition 3. Second, the MSE converges from $1 - \frac{2}{\pi}$ for $M = 1$ to $1 - \frac{\pi}{4}$, which is the limit for $M \rightarrow \infty$ as shown in Proposition 4, already at a moderate number of $M = 10$ pilots.

D. General Case

After discussing the results for the special cases, we investigate more general cases which are evaluated with numerical integration as described in Section IV-A.

First, we consider the univariate case of $N = 1$ for different numbers of observations ($M \in \{1, 2, 5, 10\}$) and with AWGN for varying SNRs in Fig. 8. For convenience, we have also plotted the closed-form solutions for the noiseless case with $M = 1$ and $M \rightarrow \infty$ as dashed lines. As expected, for $M = 1$, the CME equals the Bussgang estimator and converges to the closed-form MSE $1 - \frac{2}{\pi}$ for high SNR values. Interestingly, for an increasing number of observations there is an increasing gap between the Bussgang estimator and the CME, especially

in the mid to high SNR regime. It can also be seen that for higher numbers of observations the MSE has a minimum at a certain SNR after which it increases again. What is more, the asymptotic limit of $M \rightarrow \infty$ for infinite SNR ($\mathbf{n} \rightarrow \mathbf{0}$) can be outperformed with a finite number of observations and finite SNR. These observations, seeming counterintuitive at first, are a consequence of the *stochastic resonance* effect [41]. This is a well-known effect related to quantization where noise can improve the performance of a system with quantization. Hence, this analysis allows for a numerical quantification of the stochastic resonance effect, which is the reason why the asymptotic limit can be outperformed and thus also describes the effect of the increasing MSE after a certain SNR value. Interestingly, the influence of the stochastic resonance increases for higher numbers of pilot observations.

Next, in Fig. 9, we analyze the behavior of the Bussgang estimator and the CME for $N = 1$ and an increasing number of observations at a fixed SNR of 10dB. Similar as described before, the performance gap increases for higher numbers of observations. Whereas the MSE of the Bussgang estimator saturates with a high error floor, the MSE of the CME decreases further for higher numbers of observations.

Finally, in Fig. 10, we depict the MSE for the case of

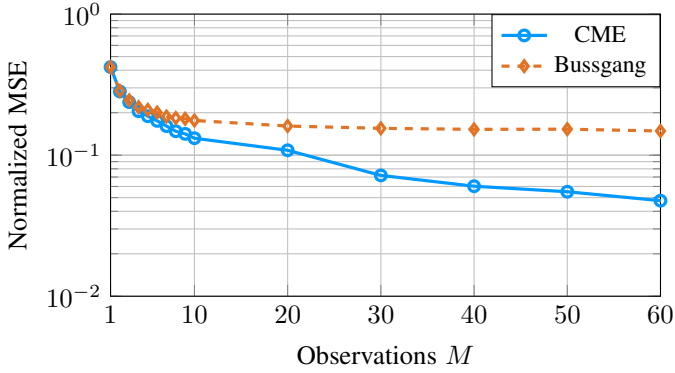


Fig. 9: MSE performance comparison between the Bussgang estimator and the CME from Section IV-A for the univariate case with SNR = 10dB.

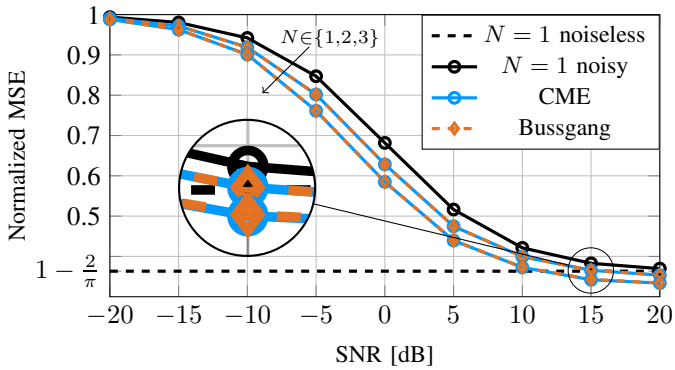


Fig. 10: MSE performance comparison between the Bussgang estimator and the CME from Section IV-A for the multivariate case with a single observation.

multiple dimensions with AWGN over the SNR for correlated channel entries. For convenience, we have also plotted the closed-form solutions for $N = 1$ with and without AWGN. Due to the exponentially increasing complexity of the numerical integration, we were only able to plot until $N = 3$ to show the tendency of the results. First, an offset of the normalized MSE for higher dimensions can be observed which seems to decrease with the number of dimensions. Moreover, the Bussgang estimator is very close to the CME which is in accordance with the prior results for low dimensions. The curve for $N = 2$ ($N = 3$) intersects with the noiseless case of $N = 1$ at about 15dB (12dB) SNR.

VII. CONCLUSION AND FUTURE WORK

In this work, we have investigated the CME for one-bit quantized systems in a jointly Gaussian setting. We derived a novel closed-form solution for multiple observations and a transformation into a computationally efficient expression where only Gaussian integrals have to be evaluated for the case without AWGN. For the general cases we conducted numerical experiments with the help of numerical integration.

Additionally, we have proposed a MSE-optimal pilot sequence which we motivated by the structure of the CME. It turned out that a successive shift of the transmit signals' angle

is optimal which was already proposed in prior work with a different motivation in the context of deep learning.

We analyzed the well-known Bussgang estimator and showed the equivalence of the Bussgang estimator and the CME in the univariate case with a single observation, which extends to the multivariate case when there is no correlation between the channel or noise entries. In addition, we showed that the closed-form MSE terms of the Bussgang estimator and the CME are equal in the case of multiple observations without AWGN. To this end, we found a closed-form expression for the inverse of the covariance matrix of the quantized observation which is derived with the arcsine law.

For the general case where numerical integration is necessary, we found that the performance gap between the Bussgang estimator and the CME increases for higher dimensions, longer pilot sequences, or higher SNR values. This observation was confirmed by the analysis of the cosine similarity and a bound on the achievable rate as different performance metrics.

The findings of this work may facilitate extensions to more general input distributions, e.g., Gaussian mixture models (GMMs), different nonlinearities such as the clipper function instead of the one-bit quantization, or to quantizers with higher resolutions.

APPENDIX

A. Proof of Proposition 1

Proof. First, it can be observed that due to the absence of noise the expression in (15) simplifies to an indicator function

$$p_{\mathbf{r}_{\mathbb{R}}|\mathbf{h}_{\mathbb{R}}}(\mathbf{r}_{\mathbb{R}}|\mathbf{h}_{\mathbb{R}}) = \begin{cases} 1, & \mathbf{h}_{\mathbb{R}} \in \bar{Q}(\mathbf{r}_{\mathbb{R}}) \\ 0, & \mathbf{h}_{\mathbb{R}} \notin \bar{Q}(\mathbf{r}_{\mathbb{R}}) \end{cases} \quad (43)$$

such that we get

$$E[\mathbf{h}_{\mathbb{R}} | \mathbf{r}_{\mathbb{R}}] = \frac{1}{p_{\mathbf{r}_{\mathbb{R}}}(\mathbf{r}_{\mathbb{R}})} \int_{\bar{Q}(\mathbf{r}_{\mathbb{R}})} \mathbf{h}_{\mathbb{R}} f_{\mathbf{h}_{\mathbb{R}}}(\mathbf{h}_{\mathbb{R}}) d\mathbf{h}_{\mathbb{R}}. \quad (44)$$

Second, we can interpret the integral in (44) as the (scaled) mean of a truncated multivariate Gaussian, i.e.,

$$\int_{\bar{Q}(\mathbf{r}_{\mathbb{R}})} \mathbf{h}_{\mathbb{R}} f_{\mathbf{h}_{\mathbb{R}}}(\mathbf{h}_{\mathbb{R}}) d\mathbf{h}_{\mathbb{R}} = p_{\mathbf{r}_{\mathbb{R}}}(\mathbf{r}_{\mathbb{R}}) E[\tilde{\mathbf{h}}_{\mathbb{R}}] \quad (45)$$

where $\tilde{\mathbf{h}}_{\mathbb{R}} \sim f_{\tilde{\mathbf{h}}_{\mathbb{R}}}$ is a truncated Gaussian RV with PDF

$$f_{\tilde{\mathbf{h}}_{\mathbb{R}}}(\tilde{\mathbf{h}}_{\mathbb{R}}) = \begin{cases} \frac{1}{p_{\mathbf{r}_{\mathbb{R}}}(\mathbf{r}_{\mathbb{R}})} \mathcal{N}(\tilde{\mathbf{h}}_{\mathbb{R}}; \mathbf{0}, \mathbf{C}_{\mathbf{h}}) & \tilde{\mathbf{h}}_{\mathbb{R}} \in \bar{Q}(\mathbf{r}_{\mathbb{R}}) \\ 0 & \tilde{\mathbf{h}}_{\mathbb{R}} \notin \bar{Q}(\mathbf{r}_{\mathbb{R}}) \end{cases} \quad (46)$$

and $p_{\mathbf{r}_{\mathbb{R}}}(\mathbf{r}_{\mathbb{R}})$ is the normalization such that $f_{\tilde{\mathbf{h}}_{\mathbb{R}}}$ is a valid PDF that integrates to one. In [48], [49], the mean of a one-sided truncated Gaussian RV is derived, which in our case is computed to

$$p_{\mathbf{r}_{\mathbb{R}}}(\mathbf{r}_{\mathbb{R}}) E[[\tilde{\mathbf{h}}_{\mathbb{R}}]_i] = \sum_{n=1}^N [\mathbf{r}_{\mathbb{R}}]_n [\mathbf{C}_{\mathbf{h}}]_{i,n} \mathcal{N}(0; 0, [\mathbf{C}_{\mathbf{h}}]_{n,n}) \int_{\bar{Q}(\mathbf{r}_{\mathbb{R}}^n)} \mathcal{N}^n(\mathbf{x}; \mathbf{0}, \mathbf{C}_{\mathbf{h}}) d\mathbf{x}. \quad (47)$$

Plugging (47) into (45) together with (44) yields the expression in (26) and thus finishes the proof. \square

$$[\mathbf{T}]_{n,n} = \begin{cases} M - \frac{M}{2}(2 - \frac{2}{M}) & 1 < n < M \\ M - \frac{M}{2}(1 - \frac{1}{M} + j\frac{1}{M}) + j\frac{M}{2}(1 - \frac{M-1}{M} + j\frac{M-1}{M}) & n = 1 \\ M - \frac{M}{2}(1 - \frac{1}{M} - j\frac{1}{M}) - j\frac{M}{2}(1 - \frac{M-1}{M} + j\frac{1-M}{M}) & n = M \end{cases} = 1. \quad (59)$$

$$[\mathbf{T}]_{m,n}^{m \neq n} = \begin{cases} M(1 - \frac{|m-n|}{M} + j\frac{m-n}{M}) - \frac{M}{2}(2 - \frac{|m-n-1|+|m-n+1|}{M} + 2j\frac{m-n}{M}) & 1 < n < M \\ M(1 - \frac{|1-n|}{M} + j\frac{1-n}{M}) - \frac{M}{2}(1 - \frac{|2-n|}{M} + j\frac{2-n}{M}) + j\frac{M}{2}(1 - \frac{|M-n|}{M} + j\frac{M-n}{M}) & n = 1 \\ M(1 - \frac{|M-n|}{M} + j\frac{M-n}{M}) - \frac{M}{2}(1 - \frac{|M-n-1|}{M} + j\frac{M-n-1}{M}) - j\frac{M}{2}(1 - \frac{|1-n|}{M} + j\frac{1-n}{M}) & n = M \end{cases} = 0. \quad (60)$$

B. Proof of Proposition 2

Proof. After plugging (27) into (12) we get

$$\mathbb{E}[h | \mathbf{r}] = \frac{1}{p_{\mathbf{r}}(\mathbf{r})} \int_{\mathcal{Q}(\mathbf{r})} h f_h(h) dh \quad (48)$$

$$= \frac{1}{\pi\sigma^2 p_{\mathbf{r}}(\mathbf{r})} \int_{\mathcal{Q}(\mathbf{r})} h e^{-\frac{|h|^2}{\sigma^2}} dh \quad (49)$$

with $\mathcal{Q}(\mathbf{r})$ from (28). Due to the symmetry of the zero-mean Gaussian PDF we get $p_{\mathbf{r}}(\mathbf{r}) = \frac{1}{4M}$ since the complex plane is divided into $4M$ circular sectors. For the integral in (49) we first transform into polar coordinates with $\Re(h) = \alpha \cos \theta$, $\Im(h) = \alpha \sin \theta$, and $dh = \alpha d\theta d\alpha$. Then, we utilize the set in (28) to find the integration limits. Due to symmetry, it is sufficient to solve for the first circular sector with $\theta \in [0, \frac{\pi}{2M}]$ and afterwards get the general solution by shifting the complex angle by $\phi(\mathbf{r})$. To this end, we compute

$$\int_0^\infty \alpha^2 e^{-\frac{\alpha^2}{\sigma^2}} \int_0^{\frac{\pi}{2M}} (\cos \theta + j \sin \theta) d\theta d\alpha$$

$$= \frac{\sqrt{\pi}\sigma^3}{4} \left(\sin\left(\frac{\pi}{2M}\right) + j \left(1 - \cos\left(\frac{\pi}{2M}\right)\right) \right) \quad (50)$$

$$= \frac{\sqrt{\pi}\sigma^3}{2} \sin\left(\frac{\pi}{4M}\right) \exp\left(j\frac{\pi}{4M}\right). \quad (51)$$

The general solution is then simply found by adding $\phi(\mathbf{r})$ in the complex exponential in (51). Finally, plugging the generalized (51) into (49) together with $p_{\mathbf{r}}(\mathbf{r}) = \frac{1}{4M}$ from above we arrive at (31) which finishes the proof. \square

C. Proof of Proposition 3

Proof. With the vector in (29), its outer product is computed as

$$[\mathbf{a}\mathbf{a}^H]_{m,n} = \exp\left(j\frac{\pi}{2M}(m-n)\right) \quad (52)$$

and thus

$$[\Re(\mathbf{a}\mathbf{a}^H)]_{m,n} = \cos\left(\frac{\pi}{2M}(m-n)\right), \quad (53)$$

$$[\Im(\mathbf{a}\mathbf{a}^H)]_{m,n} = \sin\left(\frac{\pi}{2M}(m-n)\right). \quad (54)$$

We simplify the expression for the covariance matrix from (10) as

$$\mathbf{C}_{\mathbf{r}} = \frac{2}{\pi} \left[\arcsin(\Re(\mathbf{a}\mathbf{a}^H)) + j \arcsin(\Im(\mathbf{a}\mathbf{a}^H)) \right]. \quad (55)$$

After plugging in (53) and (54) we get

$$[\mathbf{C}_{\mathbf{r}}]_{m,n} = \frac{2}{\pi} \left[\arcsin\left(\cos\left(\frac{\pi}{2M}(m-n)\right)\right) \right. \quad (56)$$

$$\left. + j \arcsin\left(\sin\left(\frac{\pi}{2M}(m-n)\right)\right) \right]$$

$$= 1 - \frac{|m-n|}{M} + j\frac{m-n}{M}. \quad (57)$$

Now, we aim to parametrize the inverse of $\mathbf{C}_{\mathbf{r}}$ with the following proposition.

Proposition 5. *The inverse of $\mathbf{C}_{\mathbf{r}}$ from (57) is given as*

$$[\mathbf{C}_{\mathbf{r}}^{-1}]_{m,n} = \begin{cases} M & m = n \\ -\frac{M}{2} & |m-n| = 1 \\ j\frac{M(n-m)}{2(M-1)} & |m-n| = M-1 \\ 0 & \text{otherwise} \end{cases}. \quad (58)$$

Proof. To prove that (58) is the inverse of (55) we define the matrix $\mathbf{T} = \mathbf{C}_{\mathbf{r}}^{-1}\mathbf{C}_{\mathbf{r}}$. If we show that \mathbf{T} is the identity matrix, i.e., $\mathbf{T} = \mathbf{I}$, then Proposition 5 holds. The m, n th element of \mathbf{T} is given as $[\mathbf{T}]_{m,n} = \sum_{l=1}^M [\mathbf{C}_{\mathbf{r}}^{-1}]_{m,l} [\mathbf{C}_{\mathbf{r}}]_{l,n}$. Due to the sparsity of $\mathbf{C}_{\mathbf{r}}^{-1}$, only three summands are non-zero. For example, we can compute $[\mathbf{T}]_{m,n}$ for $m = n = 1$:

$$[\mathbf{T}]_{1,1} = \sum_{l=1}^M [\mathbf{C}_{\mathbf{r}}^{-1}]_{1,l} [\mathbf{C}_{\mathbf{r}}]_{l,1}$$

$$= [\mathbf{C}_{\mathbf{r}}^{-1}]_{1,1} [\mathbf{C}_{\mathbf{r}}]_{1,1} + [\mathbf{C}_{\mathbf{r}}^{-1}]_{1,2} [\mathbf{C}_{\mathbf{r}}]_{2,1} + [\mathbf{C}_{\mathbf{r}}^{-1}]_{1,M} [\mathbf{C}_{\mathbf{r}}]_{M,1}$$

$$= M \cdot 1 + \left(-\frac{M}{2}\right) \cdot \left(1 - \frac{1}{M} + j\frac{1}{M}\right)$$

$$+ j\frac{M}{2} \cdot \left(1 - \frac{M-1}{M} + j\frac{M-1}{M}\right) = 1.$$

We show that the diagonal elements of \mathbf{T} , i.e., $m = n$, are one in (59) and that all off-diagonal elements of \mathbf{T} , i.e., $m \neq n$, are zero in (60). \square

With Proposition 5 we can now find the expression of

$$\mathbf{a}^H \mathbf{C}_{\mathbf{r}}^{-1} \mathbf{a} = \sum_{m=1}^M \sum_{n=1}^M [\mathbf{a}^H]_m [\mathbf{C}_{\mathbf{r}}^{-1}]_{m,n} [\mathbf{a}]_n \quad (61)$$

$$= \sum_{m=1}^M M - \frac{M}{2} \sum_{m=1}^M \left(\exp(-j\frac{\pi}{2M}) + \exp(j\frac{\pi}{2M}) \right) \quad (62)$$

$$= M^2 - M^2 \cos\left(\frac{\pi}{2M}\right) \quad (63)$$

$$= 2M^2 \sin^2\left(\frac{\pi}{4M}\right). \quad (64)$$

Plugging this into (33) results in the same MSE term as in (32) and thus finishes the proof. \square

REFERENCES

- [1] T. Cover and J. Thomas, *Elements of Information Theory*. John Wiley & Sons, Ltd, 2005.
- [2] R. Walden, "Analog-to-Digital Converter Survey and Analysis," *IEEE J. Sel. Areas Commun.*, vol. 17, no. 4, pp. 539–550, 1999.
- [3] A. Mezghani and J. A. Nossek, "Analysis of Rayleigh-Fading Channels with 1-Bit Quantized Output," in *2008 IEEE Int. Symp. Inf. Theory*, 2008, pp. 260–264.
- [4] J. A. Nossek and M. T. Ivrlač, "Capacity and Coding for Quantized MIMO Systems," in *Proc. Int. Conf. Wireless Commun. Mobile Comput.*, 2006, p. 1387–1392.
- [5] J. Mo and R. W. Heath, "High SNR Capacity of Millimeter Wave MIMO Systems with One-Bit Quantization," in *2014 Inf. Theory Appl. Workshop (ITA)*, 2014, pp. 1–5.
- [6] A. Bazrafkan and N. Zlatanov, "Asymptotic Capacity of Massive MIMO With 1-Bit ADCs and 1-Bit DACs at the Receiver and at the Transmitter," *IEEE Access*, vol. 8, pp. 152 837–152 850, 2020.
- [7] A. Mezghani and J. Nossek, "Capacity Lower Bound of MIMO Channels with Output Quantization and Correlated Noise," in *Int. Symp. Inf. Theory*, 2012.
- [8] S. Jacobsson, G. Durisi, M. Coldrey, U. Gustavsson, and C. Studer, "One-Bit Massive MIMO: Channel Estimation and High-Order Modulations," in *2015 IEEE Int. Conf. Commun. Workshop (ICCW)*, 2015, pp. 1304–1309.
- [9] Y. Li, C. Tao, G. Seco-Granados, A. Mezghani, A. L. Swindlehurst, and L. Liu, "Channel Estimation and Performance Analysis of One-Bit Massive MIMO Systems," *IEEE Trans. Signal Process.*, vol. 65, no. 15, pp. 4075–4089, 2017.
- [10] S. Jacobsson, G. Durisi, M. Coldrey, U. Gustavsson, and C. Studer, "Throughput Analysis of Massive MIMO Uplink With Low-Resolution ADCs," *IEEE Trans. Wireless Commun.*, vol. 16, no. 6, pp. 4038–4051, 2017.
- [11] M. Ivrlac and J. Nossek, "On MIMO Channel Estimation with Single-Bit Signal-Quantization," in *ITG Workshop on Smart Antennas*, 2007.
- [12] M. S. Stein, S. Bar, J. A. Nossek, and J. Tabrikian, "Performance Analysis for Channel Estimation With 1-Bit ADC and Unknown Quantization Threshold," *IEEE Trans. Signal Process.*, vol. 66, no. 10, pp. 2557–2571, 2018.
- [13] J. Choi, J. Mo, and R. W. Heath, "Near Maximum-Likelihood Detector and Channel Estimator for Uplink Multiuser Massive MIMO Systems With One-Bit ADCs," *IEEE Trans. Commun.*, vol. 64, no. 5, pp. 2005–2018, 2016.
- [14] T. Lok and V.-W. Wei, "Channel Estimation with Quantized Observations," in *1998 IEEE Int. Symp. Inf. Theory*, 1998, p. 333.
- [15] R. P. David and J. Cal-Braz, "Feedback-Controlled Channel Estimation with Low-resolution ADCs in Multiuser MIMO Systems," in *IEEE Int. Conf. Acoust., Speech, Signal Process. (ICASSP)*, 2019, pp. 4674–4678.
- [16] F. Liu, X. Shang, Y. Cheng, and G. Zhang, "Computationally Efficient Maximum Likelihood Channel Estimation for Coarsely Quantized Massive MIMO Systems," *IEEE Wireless Commun. Lett.*, vol. 26, no. 2, pp. 444–448, 2022.
- [17] F. Liu, X. Shang, and H. Zhu, "Efficient Majorization-Minimization-Based Channel Estimation for One-Bit Massive MIMO Systems," *IEEE Trans. Wireless Commun.*, vol. 20, no. 6, pp. 3444–3457, 2021.
- [18] A. Mezghani, F. Antreich, and J. A. Nossek, "Multiple Parameter Estimation with Quantized Channel Output," in *2010 Int. ITG Workshop on Smart Antennas (WSA)*, 2010, pp. 143–150.
- [19] C. Studer and G. Durisi, "Quantized Massive MU-MIMO-OFDM Uplink," *IEEE Trans. Commun.*, vol. 64, no. 6, pp. 2387–2399, 2016.
- [20] C. Stöckle, J. Munir, A. Mezghani, and J. A. Nossek, "Channel Estimation in Massive MIMO Systems using 1-Bit Quantization," in *IEEE 17th Int. Workshop Signal Process. Advances Wireless Commun. (SPAWC)*, 2016.
- [21] F. Wang, J. Fang, H. Li, Z. Chen, and S. Li, "One-Bit Quantization Design and Channel Estimation for Massive MIMO Systems," *IEEE Trans. Veh. Technol.*, vol. 67, no. 11, pp. 10 921–10 934, 2018.
- [22] N. J. Myers, K. N. Tran, and R. W. Heath, "Low-Rank mmWave MIMO Channel Estimation in One-Bit Receivers," in *2020 IEEE Int. Conf. Acoust., Speech Signal Process. (ICASSP)*, 2020, pp. 5005–5009.
- [23] L. Xu, F. Gao, and C. Qian, "Gridless Angular Domain Channel Estimation for mmWave Massive MIMO System with One-Bit Quantization via Approximate Message Passing," in *Proc. IEEE Global Commun. Conf. (GLOBECOM)*, 2019.
- [24] J. Mo, P. Schniter, and R. W. Heath, "Channel Estimation in Broadband Millimeter Wave MIMO Systems With Few-Bit ADCs," *IEEE Trans. Signal Process.*, vol. 66, no. 5, pp. 1141–1154, 2018.
- [25] Y. Dong, H. Wang, and Y.-D. Yao, "Channel Estimation for One-Bit Multiuser Massive MIMO Using Conditional GAN," *IEEE Commun. Lett.*, vol. 25, no. 3, pp. 854–858, 2021.
- [26] Y. Zhang, M. Alrabeiah, and A. Alkhateeb, "Deep Learning for Massive MIMO With 1-Bit ADCs: When More Antennas Need Fewer Pilots," *IEEE Wireless Commun. Lett.*, vol. 9, no. 8, pp. 1273–1277, 2020.
- [27] R. Zhu and G. Zhang, "A Segment-Average Based Channel Estimation Scheme for One-Bit Massive MIMO Systems with Deep Neural Network," in *Proc. IEEE Int. Conf. on Commun. Technol. (ICCT)*, 2019, pp. 81–86.
- [28] L. V. Nguyen, A. L. Swindlehurst, and D. H. N. Nguyen, "SVM-Based Channel Estimation and Data Detection for One-Bit Massive MIMO Systems," *IEEE Trans. Signal Process.*, vol. 69, pp. 2086–2099, 2021.
- [29] B. Fesl, M. Koller, N. Turan, and W. Utschick, "Learning a Low-Complexity Channel Estimator for One-Bit Quantization," in *54th Asilomar Conf. Signals, Syst., Comput.*, 2020, pp. 393–397.
- [30] J. J. Bussgang, "Crosscorrelation Functions of Amplitude-Distorted Gaussian Signals," MIT Research Lab. Electronics, Tech. Rep. 216, 1952.
- [31] R. Price, "A Useful Theorem for Nonlinear Devices Having Gaussian Inputs," *IRE Trans. Inf. Theory*, pp. 69–72, 1958.
- [32] H. E. Rowe, "Memoryless Nonlinearities With Gaussian Inputs: Elementary Results," *Bell System Technical Journal*, pp. 1519–1525, 1982.
- [33] Q. Wan, J. Fang, H. Duan, Z. Chen, and H. Li, "Generalized Bussgang LMMSE Channel Estimation for One-Bit Massive MIMO Systems," *IEEE Trans. Wireless Commun.*, vol. 19, no. 6, pp. 4234–4246, 2020.
- [34] O. T. Demir and E. Bjornson, "The Bussgang Decomposition of Nonlinear Systems: Basic Theory and MIMO Extensions [Lecture Notes]," *IEEE Signal Process. Magazine*, vol. 38, pp. 131–136, 2021.
- [35] H. Kim and J. Choi, "Channel Estimation for One-Bit Massive MIMO Systems Exploiting Spatio-Temporal Correlations," in *Proc. IEEE Global Commun. Conf. (GLOBECOM)*, 2018, pp. 1–6.
- [36] S. Rao, G. Seco-Granados, H. Pirzadeh, J. A. Nossek, and A. L. Swindlehurst, "Massive MIMO Channel Estimation With Low-Resolution Spatial Sigma-Delta ADCs," *IEEE Access*, vol. 9, pp. 109 320–109 334, 2021.
- [37] H. Lee, Y.-S. Jeon, H. Do, and N. Lee, "Concatenated MMSE Estimation for Quantized OFDM Systems," in *IEEE Int. Conf. Commun. (ICC)*, 2019.
- [38] A. Banerjee, X. Guo, and H. Wang, "On the Optimality of Conditional Expectation as a Bregman Predictor," *IEEE Trans. Inf. Theory*, vol. 51, no. 7, pp. 2664–2669, 2005.
- [39] C. Mollén, J. Choi, E. G. Larsson, and R. W. Heath, "Uplink Performance of Wideband Massive MIMO With One-Bit ADCs," *IEEE Trans. Wireless Commun.*, vol. 16, no. 1, pp. 87–100, 2017.
- [40] C.-K. Wen, C.-J. Wang, S. Jin, K.-K. Wong, and P. Ting, "Bayesian-Optimal Joint Channel-and-Data Estimation for Massive MIMO With Low-Precision ADCs," *IEEE Trans. Signal Process.*, vol. 64, no. 10, pp. 2541–2556, 2016.
- [41] M. D. McDonnell, N. G. Stocks, C. E. M. Pearce, and D. Abbott, *Stochastic Resonance: From Suprathreshold Stochastic Resonance to Stochastic Signal Quantization*. Cambridge University Press, 2008.
- [42] A. Papoulis and S. U. Pillai, *Probability, Random Variables and Stochastic Processes*. McGraw-Hill Education, 2002.
- [43] G. Jacovitti and A. Neri, "Estimation of the Autocorrelation Function of Complex Gaussian Stationary Processes by Amplitude Clipped Signals," *IEEE Trans. Inf. Theory*, vol. 40, no. 1, pp. 239–245, 1994.
- [44] A. Genz, "Numerical Computation of Multivariate Normal Probabilities," *J. of Comput. and Graphical Statist.*, vol. 1, no. 2, pp. 141–149, 1992.
- [45] P. Virtanen *et al.*, "SciPy 1.0: Fundamental Algorithms for Scientific Computing in Python," *Nature Methods*, vol. 17, pp. 261–272, 2020.
- [46] B. Hassibi and B. Hochwald, "How Much Training is Needed in Multiple-Antenna Wireless Links?" *IEEE Trans. Inf. Theory*, vol. 49, no. 4, pp. 951–963, 2003.
- [47] F. Pedregosa *et al.*, "Scikit-learn: Machine Learning in Python," *Journal of Machine Learning Research*, vol. 12, pp. 2825–2830, 2011.
- [48] G. M. Tallis, "The Moment Generating Function of the Truncated Multinomial Distribution," *Journal of the Royal Statistical Society. Series B (Methodological)*, pp. 223–229, 1961.
- [49] J. Carlinhour, "One-Dimensional Marginal Density Functions of a Truncated Multivariate Normal Density Function," *Commun. in Statist. - Theory and Methods*, vol. 19, no. 1, pp. 197–203, 1990.